A Novel Fuzzy Logic-Based Hepatic Tissues Segmentation from CT scan

Sangeeta K Siri, *Member, IAENG,* Pradeepa S C, *Member, IAENG,* Abhijith N, *Member, IAENG,* Pramod Kumar S, *Member, IAENG,* Sudha M S, *Member, IAENG,* and Baby H T, *Member, IAENG*

***Abstract*—Accurate liver segmentation has a direct impact on systematic clinical diagnosis, treatment planning, volume measurements, study of liver function, and prediction of diseases and abnormalities. Due to significant progress in medical imaging technologies, the amount of data being handled has increased considerably, creating a strong need for automated real-time segmentation techniques. The demand for automatic liver segmentation has attracted the attention of many researchers; as a result, numerous automatic liver segmentations have been proposed. However, this topic remains an open challenge because most of these algorithms fail to produce results suitable for clinical diagnosis. In this study, a novel cluster-based automatic segmentation method was developed. The primary requirements for cluster-based segmentation are the optimal number of clusters (k) and centroids. A novel framework was designed to obtain the optimal number of clusters and centroids using the Slope Variation Distribution (SVD) of the image. A trapezoidal-shaped membership was assigned to each pixel of the Computed Tomography (CT) scan. Subsequently, the liver segmentation results were improved using the median aggregator. Finally, we used a set of morphological operators to remove non-liver structures and obtain precise liver images. The precision of the proposed framework was tested using 100 CT scans of healthy livers and 40 CT scans of diseased livers. The average accuracy, average Relative Volume Disagreement (RVD), average Highest Contour Distance (HCD), average Mean Contour Difference (MCD), and average Dice Similarity Factor (DSF) were 92.01%, 5.75%,4.15mm, 2.44 mm, and 93.09%, respectively for healthy liver and 90.05%, 7.68%,9.30mm, 3.75 mm, and 85.22%, respectively for diseased liver, indicating promising efficacy. Furthermore, the minimal variance verifies the resilience of the framework. The encouraging outcomes highlight the effectiveness of our proposed framework in achieving precise liver segmentation from CT scans. These results indicate that our method has the potential to greatly enhance both the efficiency and dependability of liver imaging analysis in clinical environments. Additionally, further validation using larger datasets and benchmarking against leading techniques will help confirm the robustness and practical value of our approach.**

Manuscript received March 17, 2024; revised June 28, 2025.

Sangeeta K Siri is a Professor in the Department of Electronics and Communication Engineering at Global Academy of Technology, Bengaluru, Karnataka 560098, India (e-mail: sangeetamk28@gmail.com).

Pradeepa S C is an Assistant Professor in the Department of Electronics and Communication Engineering at Jawaharlal Nehru New College of Engineering, Shivamogga, Karnataka 577204, India (e-mail: pradeepasc@jnnce.ac.in).

Abhijith N is an Assistant Professor in the Department of Electronics and Communication Engineering at Jawaharlal Nehru New College of Engineering, Shivamogga, Karnataka 577204, India (e-mail: abhijithn@jnnce.ac.in).

Pramod Kumar S is an Associate Professor in the Department of Electronics and Communication Engineering at Jawaharlal Nehru New College of Engineering, Shivamogga, Karnataka 577204, India (corresponding author, phone: +91-9900312176; e-mail: pramod.s86@gmail.com).

Sudha M S is a Professor in the Department of Electronics and Communication Engineering at R.R. Institute of Technology, Bengaluru, Karnataka 560090, India (e-mail: sudharajoli94@gmail.com).

Baby H T is an Associate Professor in the Department of Electronics and Communication Engineering at Government Engineering College, Mosalehosahalli, Karnataka 573212, India (e-mail: babygowda@gmail.com).

***Index Terms*—Liver segmentation, fuzzy logic, CT images, slope variation distribution, membership function.**

I. Introduction

THE liver is the secretory gland as well as it is the heaviest and most massive internal organ. As a result, it serves a dual purpose in the body. It is a central and distinctive organ without which the body's tissues would quickly perish from a lack of vitality and nutrients. Whilst, the liver possesses an extraordinary ability to replace dead or damaged tissues. As a result, no mechanism or drug can make up for the loss of liver function. Because of the large volume of blood flow through it, its anatomical structure, and position in the human body, it has more tendency to develop a variety of ailments. There are about 100 liver problems, which can be brought on by toxins, infections, alcohol, heredity, an unbalanced diet, obesity, unhygienic practices, medicines, etc. The most commonly observed liver diseases in the human body are cancer, hepatitis, fatty liver, cirrhosis, viral hepatitis, hemochromatosis, and alpha-1 antitrypsin deficiency. According to the WHO, there will be 50 million cases of hepatitis C and 254 million cases of hepatitis B in 2022, and the number of fatalities from viral hepatitis is increasing. American Cancer Society has projected the following figures for primary liver cancer and intrahepatic bile duct carcinoma in the US by 2024: approximately 41, 630 new cases will be identified (13,630 in females and 28,000 in males). These cancers cause the death of approximately 29,840 persons (10,720 females and 19,120 males). The occurrence of liver cancer has risen over four times since 1980 and the disease fatality rate has more than doubled. If current trends continue, there might be a more than 55% escalation in liver cancer diagnoses or demises worldwide between 2020 and 2040. Primary liver cancer cases and deaths at different stages of development (low, medium, high, and extremely high) from 2020 to 2040 called as Human Development Index (HDI) is shown in Figure 1. Furthermore, cancers that originate in neighboring organs such as the lung, kidney, and breast, as well as other abdominal organs, particularly the rectum, colon and pancreas called secondary cancer, frequently spread to the liver during the disease. As a result, regular analysis of the liver and its lesions is performed for thorough tumor staging [1]. Owing to extensive advancements in medical modalities and their images, the utilization of computers is compulsory to handle large amounts of data. Specifically, segmentation algorithms are utilized for demarcating anatomical structures [2], and hence these algorithms are also helpful in computer-incorporated surgery, treatment scheduling, the

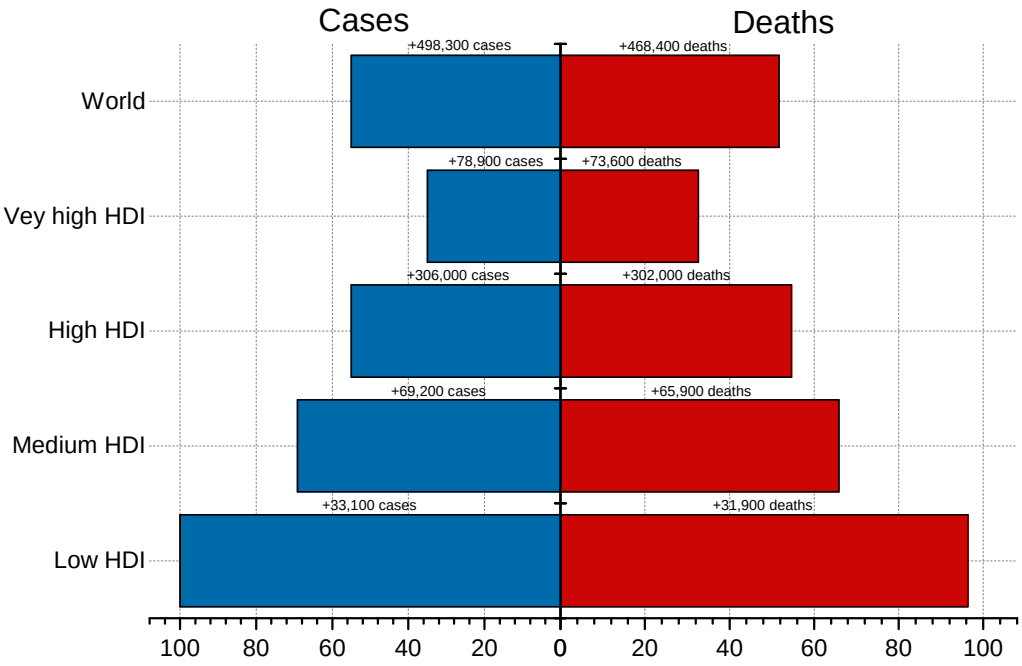

Fig. 1: Forecasted percentage change (with actual values displayed above each bar) in new cases and deaths due to primary liver cancer from 2020 to 2040, categorized by Human Development Index (HDI).

study of anatomical structures, 3D view generation, and texture analysis.

Recognizing suitable therapy for anomalous variation in liver tissues, shape analysis, treatment planning and monitoring, liver volume measurement, quantification of lesion volume, disease progression, tissue volume, and detecting pathology. Moreover, segmentation algorithms are crucial in medical image analysis such as registration, motion tracking, and labeling.

Segmenting the liver and tumors makes it simpler to calculate tumor load, which streamlines the planning process for surgical liver resection. Additionally, segmentation helps the diagnosis by precisely locating and estimating the size of the liver as well as any tumors inside its anatomical regions [3].

Medical imaging of the human body can be performed using different modalities such as X-ray, CT, ultrasound, etc. The CT scan is frequently used because of its robustness, convenience, excellent spatial resolution, and petite acquisition time.

Liver segmentation is a crucial stage that isolates the liver from abutting tissues and organs. Many articles on liver segmentation are available based on thresholding, histograms, clustering, transformation, edge detection, etc. However, these techniques are unsuccessful in delineating the liver because they rely only on pixel attributes. Many segmentation techniques fail to identify liver images accurately because their edges are fuzzy, there is high variability in both anatomical appearance and intensity pattern, inhomogeneous liver texture, unpredictable attributes, and inherent imaging noise. Moreover, the surrounding organs of the liver share similar gray levels, making delineation quite difficult. An added cause that complicates liver segmentation is the occurrence of liver pathologies, such as cancer, cirrhosis, and fatty liver.

There are three types of liver segmentation techniques: automatic, semiautomatic, and manual. The manual segmentation method provides a 100% accuracy rate and reliable output; however, it is associated with poor reproducibility and time consumption. This is reasonable for small image datasets. In many cases, manual segmentation results are used as reference images for the development of fully automatic/semiautomatic segmentation algorithms. It is also biased by intra and inter-observer variability [4].

These reasons render manual segmentation objectionable. Semi-automatic/interactive liver segmentation relies heavily on operator interactions. However, automatic liver segmentation is now in demand and does not depend on operator inputs. Over the past four decades, many researchers have attempted to design fully automatic liver segmentation; however, there remains scope for enhancing accuracy and boosting the resilience of the method.

The most commonly used liver segmentation methods can be classified as machine learning [5], [6], graph cuts [7], [8], [9], region growing [10], [11], edge detection methods [12], threshold methods [13], cluster-based methods [14], [15], watershed methods [16], and active contour methods [17]. However, it is a thought-provoking task to derive liver images from abdominal scans, particularly low-contrast scan images. Machine learning methods consider a wide range of liver topologies and features; however, they require a large dataset for training. Graph cut methods are based on graph theory, but they are partly limited by the striking bias problem, as region-growing methods are computationally efficient and easy to implement. However, they are sensitive to seed point selection and provide the best results if the objects are homogeneous. Edge-based techniques have been designed for disjoint detection. This provides good outcomes if the objects have high contrast. Despite being one of the earliest and fastest methods, threshold-based segmentation relies on the choice of threshold values to yield accurate

results that are selected manually or by the outcome of an algorithm. The watershed method is based on the topological interpretation of image boundaries, which provides over-segmentation in the presence of noise. The most commonly used liver segmentation method is the active contour model, which depends on sophisticated initialization and hinges on a precise speed function with strong contrast.

Cluster-based methods divide an image into k objects, which are homogeneous and mutually exclusive. Determining the optimal value of k is a difficult task, and defining the cost function for minimization can be problematic.

The importance of liver segmentation in the medical domain, combined with the challenges of accurately isolating the liver in CT scan images, has led to the creation of fully automated, cluster-based liver segmentation methods. A novel mathematical model has been designed based on SVD, which provides an ideal cluster count and their centroids.

This paper focuses on the design and analysis of fully automatic liver segmentation, offering an accurate and consistent outcome. The proposed framework is evaluated by comparing its results with state-of-the-art techniques and reference images provided by expert radiologists.

The paper is structured into six sections. Section I provides an introduction to the proposed work, outlining the background, existing challenges, the importance of liver segmentation, and the research objectives. Section II presents a review of related work in the area of fully automated liver segmentation. Section III, we present our fully automatic liver segmentation framework; experimental results are discussed in section IV; qualitative and quantitative analysis is performed in section V and VI respectively.

II. LITERATURE SURVEY

Deshmukh K et al. [18] designed an image segmentation built upon the Fuzzy Min-Max Neural Network (FMMNN) framework. In this study, the fuzzy entropy technique is used to determine the cluster count and a neural network is used to segment the image automatically. The proposed model is computationally inexpensive and robust. Santoso et al. [19] developed a model using the phase field method for brain tumor segmentation, achieving Dice Scores (DC) and Jaccard Indices (JI) of 0.97 and 0.95, respectively. This model integrates the Allen–Cahn equation and the Range–Kutta mathematical model to delineate brain tumors. The precise liver was separated by Xuesong Lu et al. [7] using the graph cut approach. Using the multi-atlas segmentation approach, a preliminary coarse liver image was produced for this investigation. Shape and multi-dimensional characteristics were used to create an accurate liver image with an average volume overlap of 94%. Sheng et al. [20] studied the performance of DenseNet, ResNet, U-Net, fuzzy c-means (FCM), and SegNet to delineate liver images from CT images. The experimental outcomes demonstrate that DenseNet is the best for liver segmentation, followed by ResNet. Among all, FCM exhibits the worst performance. Mubashir Ahmed et al. [21] anticipated a novel convolutional neural network (CNN) for liver demarcation. In this study, three convolution layers were utilized; each layer was traced by a max-pooling layer, and a two-way softmax was employed. A random gaussian distribution is employed to deliver preliminary weights. The proposed model was verified on the sliver07 dataset, attaining DC, JI, specificity, sensitivity, and accuracy of 0.95, 0.91, 0.99, 0.97, and 0.97, respectively. The computation of the slope difference distribution (SDD) of the image histogram was performed by Sangeeta et al. [13] to delineate the liver images from CT scans. Subsequently, SDD was utilized to obtain accurate liver from CT scans with a JC of 91%. Sangeeta et al. [22] a novel approach was introduced to transform CT scan images into the neutrosophic domain, which includes three subsets: edge, non-object, and object. The object subset specifically represents the hepatic region. Morphological operations were then applied to achieve accurate liver segmentation, resulting in an average positive detection rate of 92%. Lou Q et al. [23] used Shannon entropy to differentiate liver from CT scan images. Accurate liver images were obtained by dilation and erosion, yielding good findings with a DC of 95.12%. By creating a new speed term, D. Jayadevappa et al. [24]presented an enhanced variational level set method for medical image segmentation. The model provided a computation time of 62s. Na Tian et al. [25] anticipated a self-learning framework that takes tokenized images as inputs. This model creates a precise feature map to generate an accurate image segmentation. A deep learning architecture with leaky ReLU layers was suggested by Nayantara et al. [26] in order to retrieve accurate liver from a collection of CT scans. The 96% of the dice coefficient was attained using this framework. A novel deep-learning approach was suggested by Zhang et al. [27] that uses circular areas to extract liver images from abdominal CT scans with 95% confidence intervals and identify hepatic steatosis.

III. METHODOLOGY

A. Pre-processing stage

The CT scan image is in 1020X680 DICOM color format. Transfigure the CT image to a greyscale of size 256X256.

B. Extraction of the optimal number of clusters and centroids based on Slope Variation Distribution (SVD) of image histogram [28], [29], [30]

Let I (P) be an image with R different regions that we want to generate using the fuzzy logic method. The segmented image is achieved so that.

$S(R) = g_s\{I(P)\}$ where $g_s\{\cdot\}$ is the segmentation technique which is considered a mapping function that transforms the L gray level (0 to 255) to R values i.e. $L \longrightarrow R$ where $R \prec L$.

The proposed framework for CT image segmentation assumes that each pixel in the image I(P) will have a certain degree of membership function in each region R. The membership function is designated by $\mu_r, r = 1, 2, \ldots..R$. Spatial aggregations will be performed into the membership plan to make the relationship between surrounding pixels to obtain precise liver segmentation.

Finding the best-fitting number of clusters in an image is an important and complex step. This can be obtained manually by a trial-and-error method or an automatic technique can be designed. The initial values of the centroids and several clusters have a significant impact on the final segmentation result. Hence, a novel methodology is followed

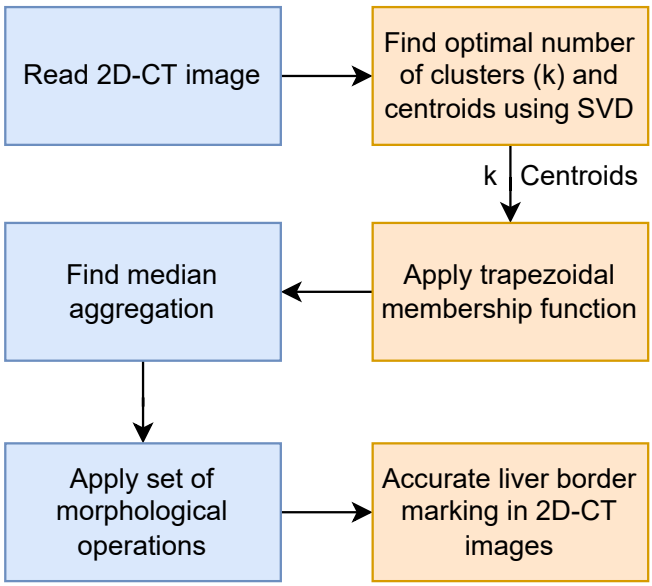

Fig. 2: Flowchart of proposed model.

to achieve the optimal number of clusters and centroids, as follows:
(i) Normalize the histogram distribution of an image as follows

$$\ddot{P}(n=i)=\frac{H_i}{H_J} \qquad i=\quad 1\quad 2\quad \ldots\ldots\ldots 256 \tag{1}$$

$$j=arg\ \underset{j\in[1,256]}{max}\ H_j$$

Greyscale frequency is denoted by H_i and maximum frequency by H_j, occurs at j in the interval [1,256].
(ii) Calculate discrete Fourier transform (DFT) of $\ddot{P}\ (n)$ as follows.

$$F(x)=\sum_{x=1}^{256}\ddot{P}(n)\,e^{-i\frac{2\Pi xn}{255}} \qquad x=1,2,\ldots.256 \tag{2}$$

(iii) Choose a low-frequency component and eliminate a high-frequency component.

$$\hat{F}(x)=\begin{cases} F(x); & x=1,2\ldots\ldots\ldots\ldots\ldots\ldots 10 \\ 0; & x=11,17,\ldots\ldots\ldots 256 \end{cases} \tag{3}$$

(iv)Transmute frequency domain to time domain as follows.

$$\tilde{P}(n)=\frac{1}{256}\sum_{x=1}^{256}\hat{F}(x)\,e^{i\frac{2\Pi xn}{255}}; \qquad x=1,\ldots..256 \tag{4}$$

$\tilde{P}(n)$ is a smoothed histogram distribution of low-frequency components ranging from 0 to 10. The range of low-frequency components is chosen by exhaustive experimentation on a varied variety of CT images. The left and right slopes of each point on the smoothed histogram distribution are distinct from one another. Fit a line model with N=5 neighboring points at each side to determine them. The formulation of the line model is as follows.

$$y_i=ax_i+b \tag{5}$$

$$[a,b]^T=(C^TC)^{-1}C^TY \tag{6}$$

$$C=\begin{bmatrix} x_1 & 1 \\ x_2 & 1 \\ . & . \\ x_{20} & 1 \end{bmatrix}\ Y=[y_1,y_2,\ldots\ldots,y_{20}]^T \tag{7}$$

(vi) The following equation provides slope variation $sv(i)$ at point i.

$$sv(i)=a_2(i)-a_1(i); \qquad i=N+1,256-N \tag{8}$$

Equation 8 yields two slopes at point i, $a_1(i)$, and $a_2(i)$.
(vii) The derivative of $sv(x)$ is equated to zero.

$$\frac{dsv(x)}{dx}=0 \tag{9}$$

(viii) Solve the above equation; we get SVD.
(ix) In SVD, crests and dips show the greatest local variation.
(x) Optimal number of clusters/Number of segmented regions(R) =Total number of crest + Total number of dips generated in SVD.
(xi) Centroid values=Intensity values of crest and dips.

C. Assigning trapezoidal-shaped membership to each pixel

A fuzzy membership function $\mu_r(x)$ with r=1, 2,.....,R is connected to each of the classes associated with centroids obtained. The membership function is formulated as in equation 10.

$$\sum_{r=1}^{R}\mu_r(I(R))=1 \tag{10}$$

At this stage, thresholding of an image can be obtained as follows.

$$T(r)=arg\,\underset{r}{max}\ \{\mu_r(I((R))\} \tag{11}$$

Using T(r), the thresholded image can be obtained. The output of this step, for each pixel, will be a vector of memberships.

$$\mu(I(R))=[\mu_1(I(P_1),\mu_2(I(P_2)\ldots.\mu_1(I(P_R)] \tag{12}$$

D. Local aggregation by median operator

The original membership function $\mu_r(I(P))$ can be modified based on local information which will provide better segmentation results. A neighbourhood $\eta(R)$ is considered, cantered around pixel p, we can utilize membership values $\mu(I(R))$ of all the pixels in $\eta(R)$ to better classify the image into R regions. The local aggregation is defined as follows.

$$\mu^S(L(R))=AG\{\mu(I(S))\} \tag{13}$$

where AG{.} is a fuzzy aggregation in a neighborhood $\eta(R)$. In this framework, median aggregation provides the best result. The memberships of each pixel in $\mu(R)$ are arrogated using the median operator.

$$\mu_r^S(I(r))=\underset{S\in\eta(r)}{median}\{\mu_r(I_r(R))\} \tag{14}$$

E. Post Processing

By performing morphological operations, a precise liver image, and its boundary is obtained from an abdominal CT scan. The flowchart of the proposed framework is described in Figure 2.

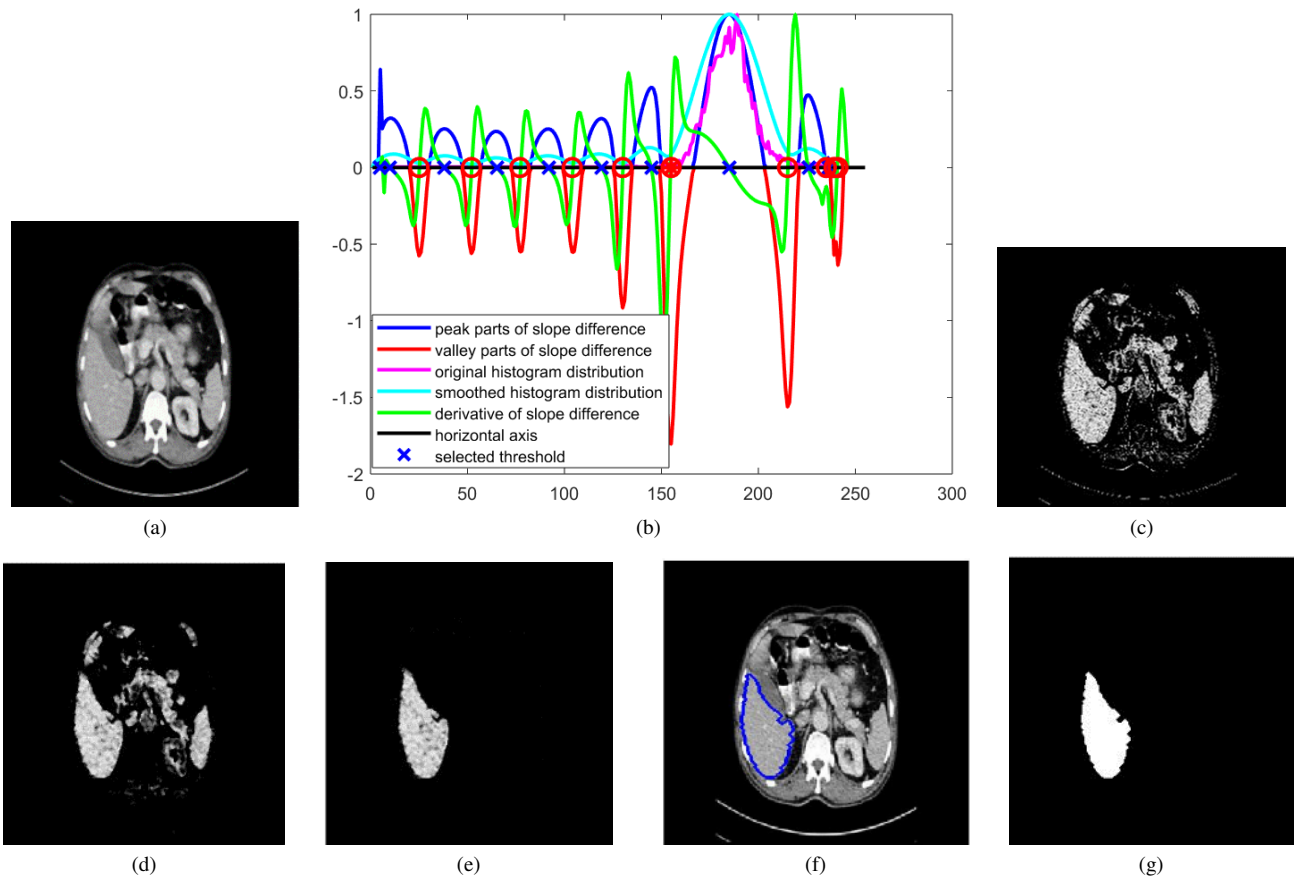

Fig. 3: Demonstration of proposed framework for healthy liver; (a) CT image; (b) Plot of peaks and dips of SVD; (c) Result of trapezoidal membership function; (d) Results of median aggregation; (e) Result of morphological operations; (f) 2D – CT scan with liver border marking. (g) Reference image.

IV. EXPERIMENTS AND RESULTS

An experimental dataset contained CT scans of 100 patients with heathy livers and 40 unhealthy livers provided by the CT Scan Center, Hubballi, Karnataka, India. Each slice of the CT image was a 1020 × 680 color image. Slice counts varied across cases, ranging from 45 to 450. The proposed fuzzy logic-based liver segmentation was realized using Matlab-R2019a.

Figure 3 shows the specifics of the anticipated model for a healthy liver. Figure 3(a) shows a 2D-CT scan image. In SVD, the largest local variation is indicated by the peaks and dips. Figure 3(b) illustrates the number of peaks, dips, and intensity values that are input to the segmentation of an image using the membership function. In this example, five peaks and five dips are generated with intensity values of [6 9 66 111 166] and [38 87 137 216 232], respectively.

The peaks are shown by blue crosses, and the dips are indicated by red circles. The intensity values of the peaks and dips are centroids for trapezoid-shaped fuzzy membership functions. Figure 3(c) shows the segmentation results based on the fuzzy membership function. Figures 3 (d) and (e) illustrate the output of median aggregation and morphological operations, respectively, to obtain a precise image of the liver from an abdominal CT scan image. Figures 3(f) and (g) illustrate a CT scan with a liver border and reference image, respectively.

Figure 4 shows the details of the proposed framework for an unhealthy liver. Figures 4(a) and (b) show a 2D-CT scan and SVD of the CT image, respectively. Figures (c) and (d) illustrate the outcome of the trapezoidal membership function and median aggregation, respectively. Figures 4(e) and (f) explain the results of morphological operations and liver boundary marking in a 2D-CT scan, respectively. Figure 4(g) demonstrates the reference image.

The number of centroids and their intensity values have a significant impact on specific liver segmentation. The proposed framework offers several clusters (K) and their centroids, providing precise CT scan liver segmentation results.

V. QUALITATIVE ANALYSIS

The outcome of the proposed method is compared with the following segmentation method:

(a) Fuzzy-c-Means (FCM) [28]
(b) K-means [28]
(c) Otsu segmentation [29]
(d) EM segmentation [30]
(e) Texture-based segmentation [31]
(f) Region-based segmentation method [32]
(g) Neutrosophic set-based segmentation [22], [33]
(h) Multi threshold-based segmentation [13]
(i) Histogram based segmentation [34]

The comparison results of the proposed framework with the state-of-the-art is illustrated in Figure 5. Figure 5, row

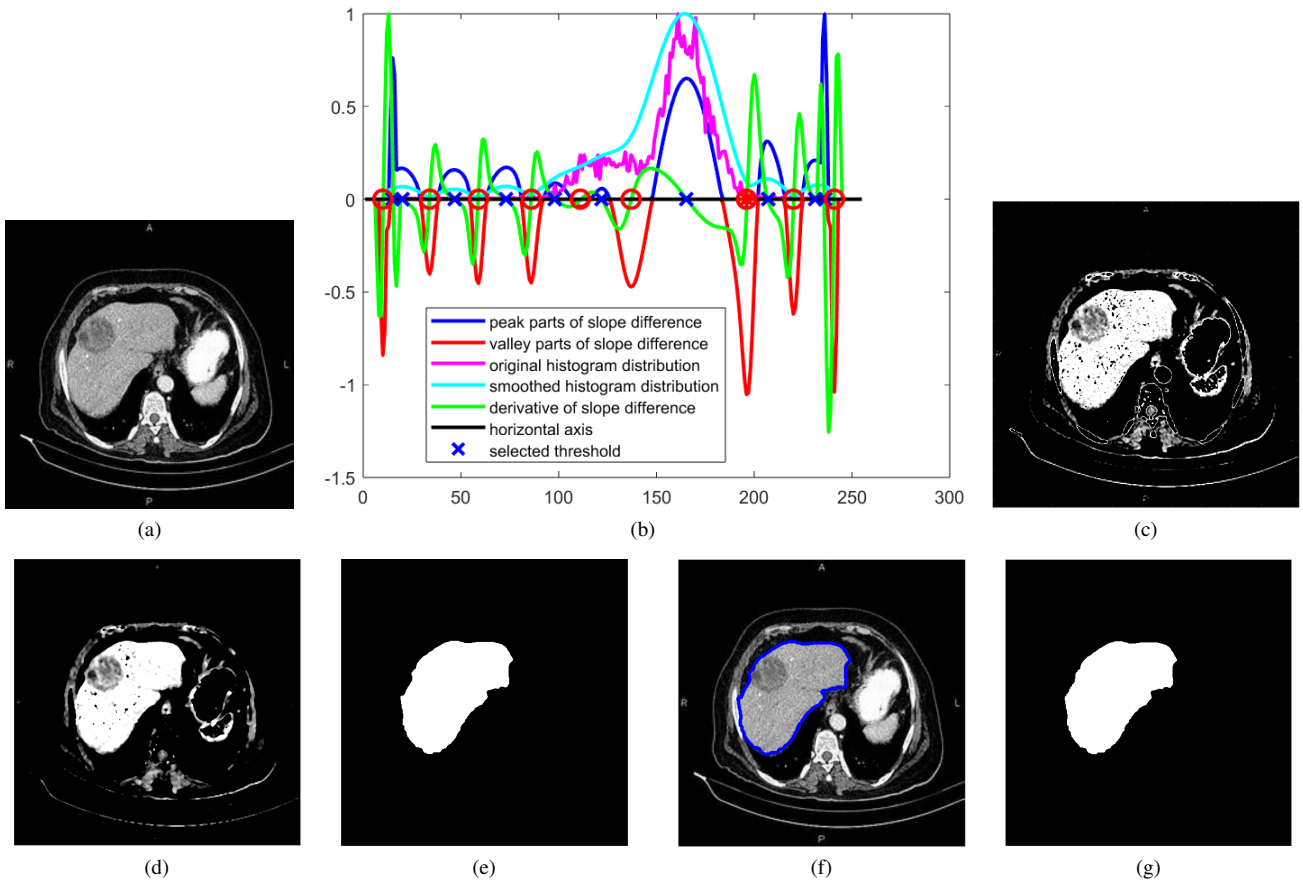

Fig. 4: Demonstration of proposed framework for diseased liver; (a) CT image; (b) Plot of peaks and dips of SVD; (c) Result of trapezoidal membership function; (d) Results of median aggregation; (e) Result of morphological operations; (f) 2D – CT scan with liver border marking. (g) Reference image.

(a) represents the 2D-CT image; row (b) illustrates the FCM results; row (c) describes the K-means algorithm results; row (d) explains Otsu segmentation results; row (e) shows EM segmentation results; row (f) represents the texture-based segmentation method; row (g) shows the region-based segmentation method; row (h) illustrates neutrosophic set-based segmentation; row (i) explains multi-threshold-based segmentation; and row (j), row (k), and row(l) show histogram-based segmentation results, proposed model outcomes, and reference images, respectively.

The visual comparison presented in Figure 5 demonstrates the effectiveness of various segmentation techniques applied to 2D-CT images. The outcomes of the proposed model, shown in row (k), can be directly compared to the reference images in row (l), allowing for a comprehensive evaluation of its performance. This side-by-side comparison enabled a clear assessment of how the proposed framework stands up against established segmentation methods, highlighting its potential advantages in accurately identifying and outlining structures in medical imagery.

VI. Quantitative Analysis

The first step in biomedical image processing is segmentation. In illness diagnosis and medication planning, a segmentation approach with high precision is a major objective because it has an impact on medical insights, such as observing tumour growth patterns. Therefore, it is crucial to evaluate the effectiveness of this segmentation method [33]. The image segmentation evaluation method compares two segmentation results by measuring how similar or different they are from one another; the first image represents the output of the segmentation technique, and the second represents the corresponding ground truth segmentation image obtained under the guidance of radiologists. Accuracy, HCD, MCD and RVD were the metrics used to evaluate the proposed model.

A. Accuracy (ACC)

Segmentation accuracy (ACC) evaluates the difference between the ground truth image and the predicted segmentation image. In this study, the ground truth image is validated using a manually segmentation under a medical practitioner's guidance. The ACC score reflects how well the algorithm's prediction aligns with the ground truth image. This evaluation metric is determined using equation [35]. According to equation 15, a perfect segmentation would result in an ACC value of 100. As the ACC value deviates from 100, it indicates a discrepancy in the segmentation. It is defined as follows.

$$ACC = \frac{Correctly\ Predicted\ Pixels}{Total\ number\ of\ image\ pixels} * 100 \quad (15)$$

Benchmarking our model against state-of-the-art algorithms using accuracy is described in Figure 6(a) and 7(a) for healthy liver and unhealthy liver respectively.

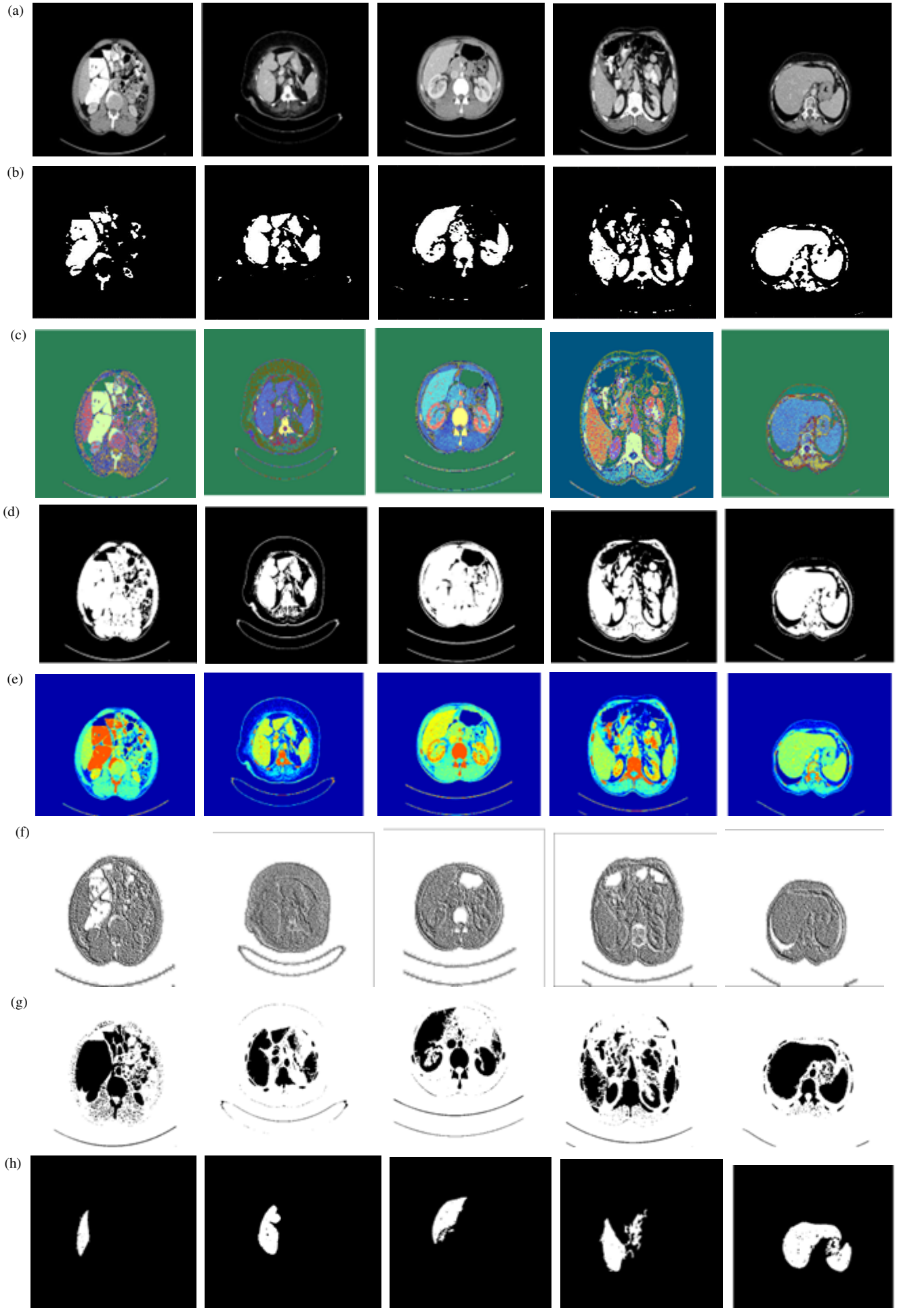

Fig. 5

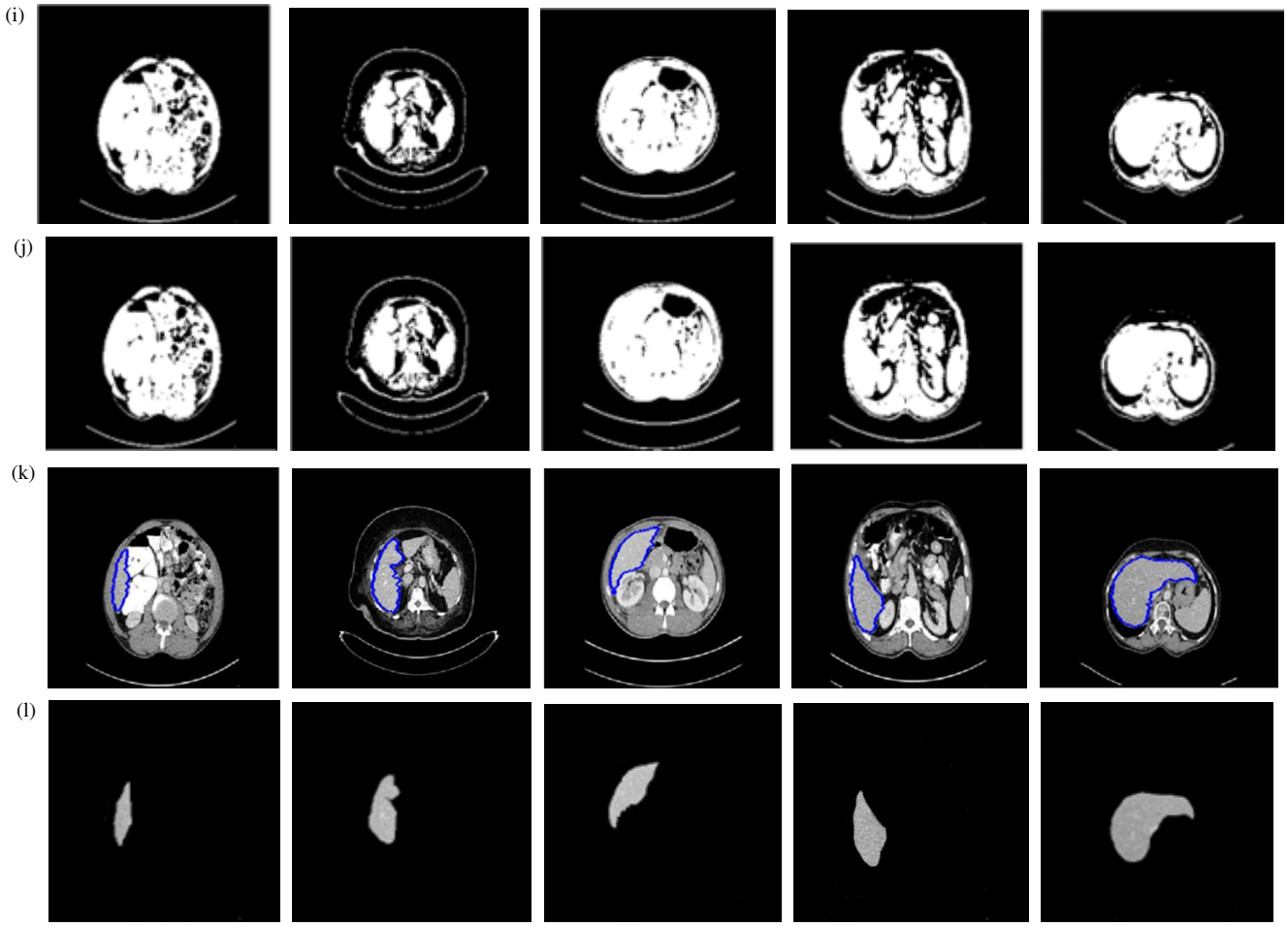

Fig. 5: Comparison results of the proposed framework with state-of-art; row (a) 2D-CT image; row (b) FCM results; row (c) K-means algorithm results; row (d) Otsu segmentation results; row (e) EM segmentation results; row (f) texture based segmentation method; row (g) region-based segmentation method; row (h) Neutrosophic set based segmentation; row (i) Mult threshold-based segmentation; row (j) histogram-based segmentation; row (k) proposed model outcomes; row(l) reference image.

B. Relative Volume Disagreement (RVD)

The specific RVD that exists between 2 images SEG_{ALG} and SEG_{GT} is given in percent and defined as.

$$RVD = 100 * (\mid SEG_{ALG} - SEG_{GT} \mid)/SEG_{GT} \quad (16)$$

With SEG_{ALG} as an image segmented by the proposed algorithm and SEG_{GT} as a ground truth image. A score of 0% indicates that the two areas completely overlap [36]. A performance comparison between the suggested model and state-of-the-art approaches using RVD is shown in Figure 6(b) and 7(b) for healthy liver and unhealthy liver respectively.

C. Highest Contour Distance (HCD)

This is the greatest gap, measured in Euclidean distances, between the set of edge pixels in the reference liver images and algorithm-segmented liver images. It was measured in mm [22], [37]. Segmentation with an HCD of 0 mm is desirable. A suggested model is compared with existing state-of-the-art methods using HCD is revealed in Figure 6(c) and 7(c) for healthy liver and unhealthy liver respectively. The HCD can be written as.

$$HCD = \max[\ dist(SEG\_ALG, SEG\_GT), dist(SEG\_GT, SEG\_ALG)] \quad (17)$$

D. Mean Contour Difference (MCD)

MCD is a mean of all the distances from the border of algorithm segmented image $SEG_{ALG}$to the border of ground truth SEG_{GT} [24] . It is formulated as follows.

$$MCD = \frac{1}{|SEG_{ALG}| + |SEG_{GT}|} * \left[\sum_{m \in SEG_{ALG}} d\left(m, SEG_{GT}\right) + \sum_{n \in SEG_{GT}} d\left(n, SEG_{ALG}\right) \right] \quad (18)$$

This will properly break the equation into two lines while maintaining readability and alignment. Where $d\left(n, SEG_{ALG}\right)$ Denotes Euclidean distance between n and SEG_{ALG}. A comparative study of the state-of-art methods and the proposed model using MCD is shown in Figure 6(d) and 7(d) for healthy liver and unhealthy liver respectively.

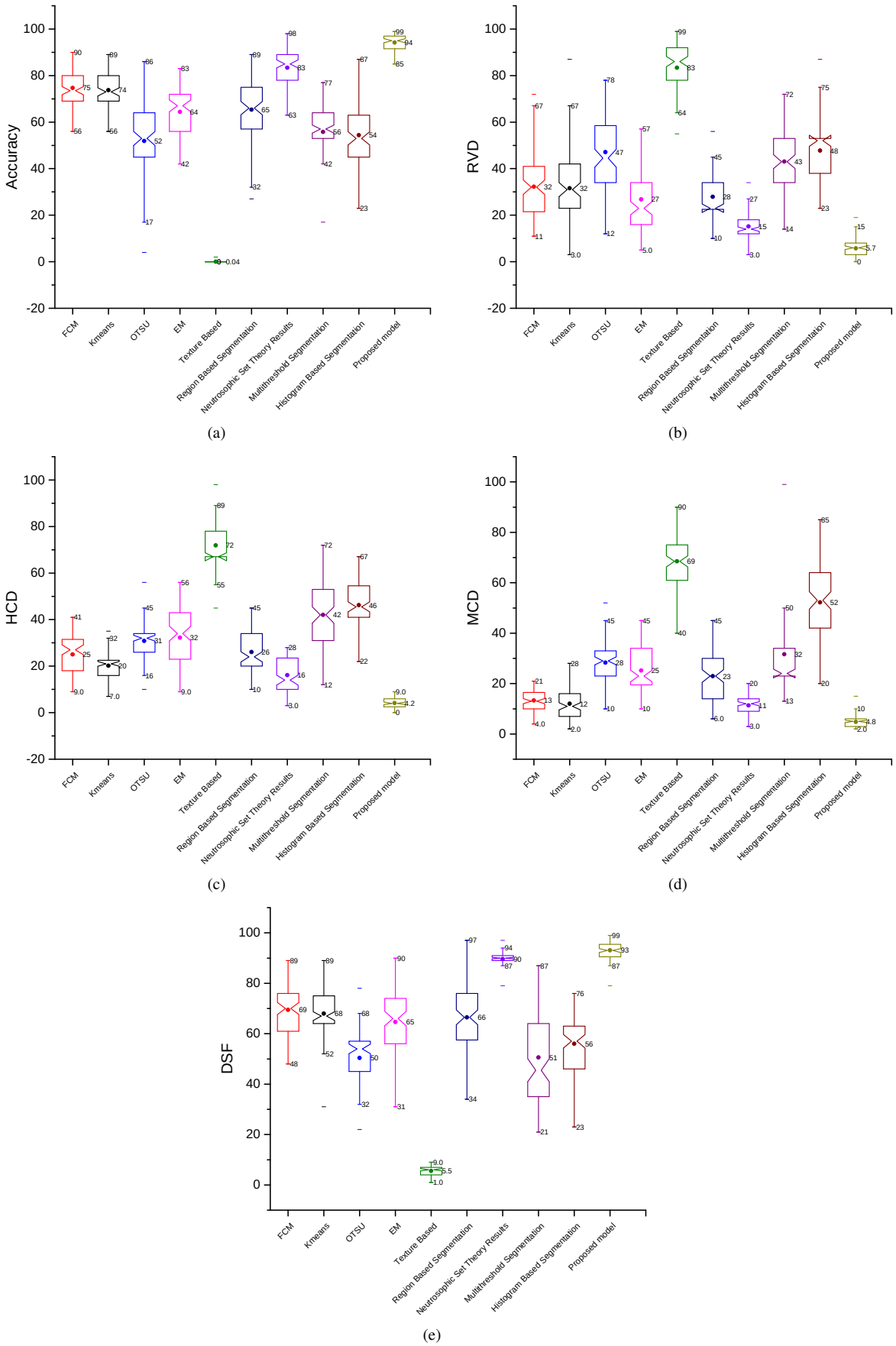

Fig. 6: Analysis of proffered framework with state-of-art techniques for healthy liver.

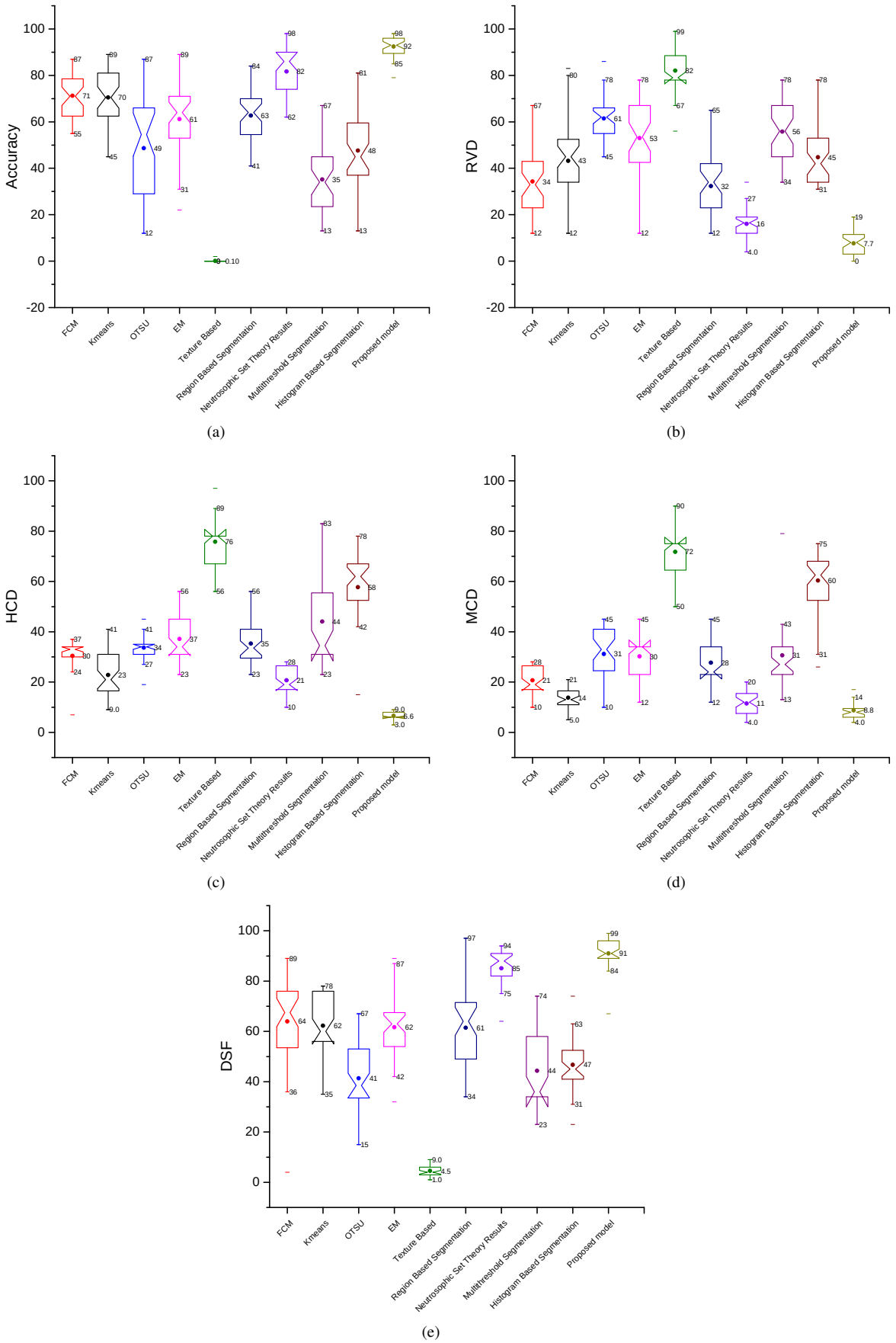

Fig. 7: Analysis of proffered framework with state-of-art techniques for liver with ailments.

TABLE I: COMPARISON OF AVERAGE METRIC VALUES FOR DIFFERENT SEGMENTATION IN EVALUATING A HEALTHY LIVER.

Method	ACC	RVD	HCD	MCD	DSF
FCM	74.69	31.15	24.99	13.29	69.43
K-means	73.73	31.54	20.2	11.97	68.04
Otsu	51.86	47.13	30.83	28.28	50.39
EM	64.39	31.62	32.26	25.17	64.65
Texture based segmentation	0.04	83.39	71.92	68.92	5.53
Region-based segmentation	65.32	27.90	26.04	22.95	66.47
Neutrosophic set results	83.39	15.19	16.15	11.35	90.65
Multithreshold segmentation	55.77	43.02	41.99	31.6	50.6
Histogram based segmentation	54.39	47.73	46.24	52.2	56.03
Proposed model	94.2	5.75	4.15	4.82	93.09

TABLE II:COMPARISON OF AVERAGE METRIC VALUES FOR DIFFERENT SEGMENTATION IN EVALUATING A UN-HEALTHY LIVER.

Method	ACC	RVD	HCD	MCD	DSF
FCM	71.25	34.28	30.43	20.7	63.95
K-means	70.5	43.73	22.8	13.75	62.23
Otsu	48.68	61.45	33.65	31.18	41.35
EM	61.13	36.33	37.15	30.23	61.68
Texture based segmentation	0.10	82.08	75.75	71.75	4.50
Region-based segmentation	62.7	34.96	35.32	27.7	61.42
Neutrosophic set results	81.7	16.08	20.7	11.48	85.08
Multithreshold segmentation	35.18	55.78	44.05	30.63	44.35
Histogram based segmentation	47.62	44.78	57.67	60.32	46.7
Proposed model	92.43	7.68	6.6	8.78	91

E. Dice Similarity Factor (DSF)

Similarity assessment is performed using the DSF, which involves computing the dice coefficient to determine the overlap between the predicted and reference objects. [38]. DSF is defined as

$$DSF = 2 * \frac{[SEG_{ALG} \cap SEG_{GT}]}{[SEG_{ALG} - SEG_{GT}]} * 100 \qquad (19)$$

where SEG_{ALG} refers to the segmentation output, while SEG_{GT} represents the corresponding ground truth. The DSF values range from 0% to 100%. A score close to 0% indicates that the segmented and ground truth areas are less or not comparable. More similarity exists between the segmented and ground truth areas if the DSF value is close to 100%. A qualified study of the state-of-the-art methods and the proposed model using DSF is depicted in Figure 6(e) and 7(e) for healthy liver and unhealthy liver respectively.

The comparison of average accuracy, RVD, HCD, MCD, and DSF for the proposed model, k-means, FCM, Otsu method, EM method, a texture-based segmentation method, region-based segmentation method, neutrosophic set-based segmentation, multi-threshold-based segmentation, and histogram-based segmentation method for healthy liver and unhealthy liver are tabulated in table I and table II respectively.

VII. CONCLUSIONS

It is challenging to analyse and anticipate liver disorders in short time in the field of liver health care because physicians must review large amounts of images produced by imaging modalities, including CT, MRI, and PET. Advanced techniques for automated liver segmentation are important for the success of computer-aided disease diagnosis (CAD) systems, as precise segmentation of the liver authorizes superior exploration and more accurate diagnosis. The proposed number of centroids and their intensity values are used as inputs for fuzzy-based segmentation. The application of median aggregation results in a coarse liver image. Finally, a set of morphological operations offers specific liver images from abdominal CT scans. The proposed model is suitable for clinical purposes because there is less variability in border distance and volume overlap. The evaluation is carried out using accuracy, RVD, MCD, and HCD, and we conclude that the proposed model provides a minimum error. This segmentation approach incorporates fuzzy logic and morphological operations to enhance the liver image extraction from abdominal CT scans. The effectiveness of the method was demonstrated through its minimal border distance variability and high-volume overlap, making it particularly suitable for clinical applications. The evaluation metrics, including accuracy, RVD, MCD, and HCD, further validated the model's performance by showing minimal error rates compared to other techniques.

REFERENCES

[1] H. Rumgay, M. Arnold, J. Ferlay, O. Lesi, C. J. Cabasag, J. Vignat, M. Laversanne, K. A. McGlynn, and I. Soerjomataram, "Global burden of primary liver cancer in 2020 and predictions to 2040," Journal of Hepatology, vol. 77, no. 6, pp. 1598–606, Dec. 2022.

[2] P. Bilic, P. Christ, H. B. Li, E. Vorontsov, A. Ben-Cohen, G. Kaissis, A. Szeskin, C. Jacobs, G. E. Mamani, G. Chartrand, and F. Lohöfer, "The liver tumor segmentation benchmark (lits)," Medical Image Analysis, vol. 84, p. 102680, Feb. 2023.

[3] S. Gul, M. S. Khan, A. Bibi, A. Khandakar, M. A. Ayari, and M. E. Chowdhury, "Deep learning techniques for liver and liver tumor segmentation: A review," Computers in Biology and Medicine, vol. 147, p. 105620, Aug. 2022.

[4] I. R. I. Haque and J. Neubert, "Deep learning approaches to biomedical image segmentation," Informatics in Medicine Unlocked, vol. 18, p. 100297, 2020.

[5] P. Hu, F. Wu, J. Peng, P. Liang, and D. Kong, "Automatic 3d liver segmentation based on deep learning and globally optimized surface evolution," Physics in Medicine and Biology, vol. 61, no. 24, p. 8676, 2016.

[6] X. Fang, S. Xu, B. J. Wood, and P. Yan, "Deep learning-based liver segmentation for fusion-guided intervention," International Journal of Computer Assisted Radiology and Surgery, vol. 15, no. 6, pp. 963–972, 2020.

[7] X. Lu, Q. Xie, Y. Zha, and D. Wang, "Fully automatic liver segmentation combining multi-dimensional graph cut with shape information in 3d ct images," Scientific Reports, vol. 8, no. 1, pp. 1–9, 2018.

[8] M. Liao, Y.-q. Zhao, W. Wang, Y.-z. Zeng, Q. Yang, F. Y. Shih, and B.-j. Zou, "Efficient liver segmentation in ct images based on graph cuts and bottleneck detection," Physica Medica, vol. 32, no. 11, pp. 1383–1396, 2016.
[9] M. Liao, Y.-q. Zhao, X.-y. Liu, Y.-z. Zeng, B.-j. Zou, X.-f. Wang, and F. Y. Shih, "Automatic liver segmentation from abdominal ct volumes using graph cuts and border marching," Computer methods and programs in biomedicine, vol. 143, pp. 1–12, 2017.
[10] S. A. Elmorsy, M. A. Abdou, Y. F. Hassan, and A. Elsayed, "A region growing liver segmentation method with advanced morphological enhancement," in 2015 32nd National Radio Science Conference (NRSC). IEEE, 2015, pp. 418–425.
[11] L. Xu, Y. Zhu, Y. Zhang, and H. Yang, "Liver segmentation based on region growing and level set active contour model with new signed pressure force function," Optik, vol. 202, p. 163705, 2020.
[12] W. Peng and Y. Zhao, "Liver ct image segmentation based on modified canny algorithm," in 2019 12th International Congress on Image and Signal Processing, BioMedical Engineering and Informatics (CISP-BMEI). IEEE, 2019, pp. 1–5.
[13] S. K. Siri, S. P. Kumar, and M. V. Latte, "Threshold-based new segmentation model to separate the liver from ct scan images," IETE Journal of Research, pp. 1–8, 2020.
[14] A.-R. Ali, M. Couceiro, A. E. Hassanien, M. F. Tolba, and V. Snášel, "Fuzzy c-means based liver ct image segmentation with an optimum number of clusters," in Proceedings of the Fifth International Conference on Innovations in Bio-Inspired Computing and Applications IBICA 2014. Springer, Cham, 2014, pp. 131–139.
[15] J. Cai, "Segmentation and diagnosis of liver carcinoma based on adaptive scale-kernel fuzzy clustering model for ct images," Journal of Medical Systems, vol. 43, no. 11, p. 322, 2019.
[16] H. Masoumi, A. Behrad, M. A. Pourmina, and A. Roosta, "Automatic liver segmentation in mri images using an iterative watershed algorithm and artificial neural network," Biomedical signal processing and control, vol. 7, no. 5, pp. 429–437, 2012.
[17] A. Biswas, P. Bhattacharya, and S. P. Maity, "An efficient semiautomatic active contour model of liver tumor segmentation from ct images," in Computational Network Application Tools for Performance Management. Springer, Singapore, 2020, pp. 75–85.
[18] S. G. Deshmukh K, "Adaptive color image segmentation using fuzzy min-max clustering," Engineering letters, vol. 13, no. 2, pp. 57–64, 2006.
[19] S. AJ, "Medical image segmentation using phase-field method based on gpu parallel programming," Engineering letters, vol. 30, no. 1, pp. 214–220, 2022.
[20] V. S. Sheng, Y. Shen, L. Wang, W. Fang, X. Xi, and D. Zhang, "Empirical comparisons of deep learning networks on liver segmentation," Computers, Materials and Continua, vol. 62, no. 3, pp. 1233–1247, 2020.
[21] M. Ahmad, Y. Ding, S. F. Qadri, and J. Yang, "Convolutional-neural-network-based feature extraction for liver segmentation from ct images," in Eleventh International Conference on Digital Image Processing (ICDIP 2019), vol. 11179. International Society for Optics and Photonics, 2019, p. 1117934.
[22] S. K. Siri and M. V. Latte, "A novel approach to extract exact liver image boundary from abdominal ct scan using neutrosophic set and fast marching method," Journal of Intelligent Systems, vol. 28, no. 4, pp. 517–532, 2019.
[23] Q. Y. Lou Q, Lin T and L. F, "Semi-supervised liver segmentation based on local regions self-supervision," Medical Physics, vol. 51, no. 5, pp. 3455–63, May 2024.
[24] K. S. Jayadevappa D and M. DS, "A new deformable model based on level sets for medical image segmentation," IAENG International Journal of Computer Science, vol. 36, no. 3, pp. 199–207, 2009.
[25] Z. W. Tian N, "East: Extensible attentional self-learning transformer for medical image segmentation," IAENG International Journal of Computer Science, vol. 50, no. 3, pp. 1021–1030, Sep. 2023.
[26] P. V. Nayantara, S. Kamath, R. Kadavigere, and K. N. Manjunath, "Automatic liver segmentation from multiphase ct using modified segnet and aspp module," SN Computer Science, vol. 5, no. 4, p. 377, 2024.
[27] Z. Zhang, G. Li, Z. Wang, F. Xia, N. Zhao, H. Nie, Z. Ye, J. S. Lin, Y. Hui, and X. Liu, "Deep-learning segmentation to select liver parenchyma for categorizing hepatic steatosis on multinational chest ct," Scientific Reports, vol. 14, no. 1, p. 11987, 2024.
[28] S. N. Madhukumar S, "Evaluation of k-means and fuzzy c-means segmentation on mr images of the brain," The Egyptian Journal of Radiology and Nuclear Medicine, vol. 46, no. 2, pp. 475–479, Jun. 2015.
[29] Z. L. Gao K, Dong M and G. M, "Image segmentation method based upon otsu aco algorithm," in Information and Automation: International Symposium, ISIA 2010, Guangzhou, China, November 10-11, 2010. Revised Selected Papers 2011. Springer Berlin Heidelberg, 2011, pp. 574–580.
[30] S. K. Siri, S. P. Kumar, and M. V. Latte, "An improved expectation-maximization algorithm to detect liver image boundary in ct scan images," IETE Journal of Research, vol. 69, no. 10, pp. 6846–54, Oct. 2023.
[31] Z. J and N. HH, "Texture-based segmentation of road images," in Proceedings of the Intelligent Vehicles' 94 Symposium. IEEE, Oct. 1994, pp. 260–265.
[32] A. FM, "A study of region-based and contour-based image segmentation," Signal and Image Processing, vol. 3, no. 6, pp. 15–22, Dec. 2012.
[33] Z. Wang, "A new approach for segmentation and quantification of cells or nanoparticles," IEEE Transactions on Industrial Informatics, vol. 12, no. 3, pp. 962–971, 2016.
[34] J. S. Bhargavi K, "A survey on threshold-based segmentation technique in image processing," International Journal of Innovative Research and Development, vol. 3, no. 12, pp. 234–9, Nov. 2014.
[35] L. M. Siri SK, "The combined endeavor of the neutrosophic set and chan-vese model to extract accurate liver images from ct scan," Computer methods and programs in biomedicine, vol. 151, pp. 101–9, Nov. 2017.
[36] J. MacQueen, "Some methods for classification and analysis of multivariate observations," in Proceedings of the Fifth Berkeley Symposium on Mathematical Statistics and Probability, Volume 1: Statistics, vol. 5. University of California press, 1967, pp. 281–298.
[37] A. A. Taha and A. Hanbury, "Metrics for evaluating 3d medical image segmentation: analysis, selection, and tool," BMC Medical Imaging, vol. 15, no. 1, pp. 1–28, 2015.
[38] D. S. Das N, "Attention-unet architectures with pretrained backbones for multi-class cardiac mr image segmentation," Current Problems in Cardiology, vol. 49, no. 1, p. 102129, Jan. 2024.

Sangeeta K Siri (M'24) completed her Bachelor of Engineering at SDMCET, Dharwad, Karnataka, India. She earned her Master's degree in Electronics from BMS College of Engineering (BMSCE), Bangalore, Karnataka, India, and was awarded a Ph.D. from Visvesvaraya Technological University (VTU), Belagavi, Karnataka, India. She is currently working as a Professor in the Department of Electronics and Communication at Global Academy of Technology (GAT), Bengaluru, Karnataka, India. Her areas of interest include image processing and pattern recognition. She received the "Best Paper" award at the National Conference on Networking, Embedded and Wireless Systems (NEWS 2010), held at BMS College of Engineering, Bangalore.

Pradeepa S C (M'24) is currently working as an Assistant Professor in the Department of Electronics and Communication at JNN College of Engineering, Shivamogga, Karnataka, India. He has 12 years of teaching experience. His areas of interest include VLSI design, embedded systems, and microcontroller programming. He is currently pursuing a Ph.D. in the field of Wireless Sensor Networks (WSNs).

Abhijith N (M'24) is currently working as an Assistant Professor in the Department of Electronics and Communication at JNN College of Engineering, Shivamogga, Karnataka, India. He has 14 years of teaching experience. His areas of interest include image processing, VLSI design, embedded systems, and microcontroller programming. He is currently pursuing a Ph.D. in the field of WSNs.

Pramod Kumar S (M'19) completed his B.E. degree in Electronics and Communication Engineering from VEC, Bellary, and his M.Tech. in VLSI Design and Embedded Systems from UTL Technologies Limited, Bangalore. He received his Ph.D. from VTU-RRC, Belagavi, Karnataka, India. He is currently working as a faculty member in the Department of Electronics and Communication at JNN College of Engineering, Shivamogga, Karnataka, India.

Sudha M S (M'24) is currently working as a Professor at R.R. Institute of Technology, Bengaluru, Karnataka, India. She is a member of IEEE, affiliated with the Circuits and Systems Society. She has published research articles in various indexed journals and has attended and presented papers at IEEE conferences. She has also filed and published several patents for innovative work carried out in collaboration with her students.

Baby H T (M'24) is currently working as an Associate Professor at Government Engineering College, Mosalehosahalli, Hassan, Karnataka, India. She has 21 years of teaching experience in various esteemed institutions. She completed her M.Tech. in Digital Communication and Networking at SJCIT, Chickballapur, in 2005, and received her Ph.D. from Visvesvaraya Technological University (VTU) in 2021. Her areas of interest include cryptography, information theory and coding, network security, and image processing.